Characterization of Enzymatically Synthesized Titania Thin Films Using Positron Annihilation Spectroscopy Reveals Low-Cost Approach for Organic/Inorganic Photovoltaic Cells

van Amelrooij, Edward F.; Schut, Henk; Egger, Werner; Dickmann, Marcel; Hugenschmidt, Christoph; Mallée, Lloyd; Hanefeld, Ulf; McMillan, Duncan G.G.; Eijt, Stephan W.H.

Important note
To cite this publication, please use the final published version (if applicable).
Please check the document version above.

Characterization of Enzymatically Synthesized Titania Thin Films Using Positron Annihilation Spectroscopy Reveals Low-Cost Approach for Organic/Inorganic Photovoltaic Cells

Edward F. van Amelrooij, Henk Schut, Werner Egger, Marcel Dickmann, Christoph Hugenschmidt, Lloyd Mallée, Ulf Hanefeld, Duncan G. G. McMillan,* and Stephan W. H. Eijt*

A new method is developed to produce mesoporous titania thin films at room temperature using the enzyme papain in a dip-coating procedure, providing low-cost titania films in a sustainable manner. Quartz crystal microbalance, positron annihilation Doppler broadening and lifetime spectroscopy, scanning electron microscopy, and X-ray diffraction are used to determine the deposition and structural properties of the films. As-deposited films have low densities $\rho \approx 0.6$ g cm^{-3}, contain small micropores and proteins, and exhibit corrugated surfaces. Annealing at temperatures of 300 °C or higher leads to the destruction and evaporation of most of the organic material, resulting in a thickness decrease of 50–60%, more pure titania films with increased density, an increase in micropore size and a decrease in the concentration and size of atomic-scale vacancies. Up to 50 layers could be stacked, allowing easy control over the total layer thickness. Based on these titania films, first test devices consisting of natural dye-sensitized solar cells are produced, that show photovoltaic activity and indicate possibilities for low-cost, accessible, organic production of solar cells. Given the wide range of other applications for titania, this new method is a promising candidate for improving the fabrication of those products with respect to cost, sustainability, and production speed.

1. Introduction

Titania thin films are a key constituent of dye-sensitized solar cells (DSSCs) and perovskite thin film solar cells, where they function as highly efficient electron transport layers. Moreover, titania films are highly relevant for application in a wide range of technologies including other photovoltaic devices, lithium-ion batteries, and protective coatings.[1,2] However, conventional methods to fabricate titania films, such as thermal oxidation, chemical vapor deposition, and electron beam physical vapor deposition, usually demand high temperature, (ultra-)high vacuum using specialized devices, or toxic environments. Such high cost production methods are often only accessible in specialized institutes,[3,4] and are often nontransferable to developing countries. In order to enhance the scale and availability of sustainable energy technologies, there is a strong need for cheap and scalable fabrication methods to produce metal oxide functional thin films, such as TiO$_2$ and ZnO electron transport layers (ETLs),[5,6] while operating in nontoxic and low-temperature environments. In search for alternative production methods, several techniques have been explored regarding the formation of metal oxide crystals from aqueous solutions using for example small molecules,[7] short polypeptides,[8] adhesive proteins,[9] and carbohydrates.[10–12] Enzymes natively function in aqueous solutions at low temperatures, and have enormous potential to achieve natural, low-temperature biomineralization. This is proven by the mineralization process provided by the enzyme silicatein.[13,14] This enzyme is present in marine sponges where it produces the silica elements in their structure, but it can also be used to generate

E. F. van Amelrooij, Dr. H. Schut, Dr. S. W. H. Eijt
Department of Radiation Science and Technology
Delft University of Technology
Mekelweg 15, NL-2629 JB Delft, The Netherlands
E-mail: s.w.h.eijt@tudelft.nl

The ORCID identification number(s) for the author(s) of this article can be found under https://doi.org/10.1002/adsu.202000003.

E. F. van Amelrooij, L. Mallée, Prof. U. Hanefeld, Dr. D. G. G. McMillan
Department of Biotechnology
Delft University of Technology
Van der Maasweg 9, NL-2629 HZ Delft, The Netherlands
E-mail: d.g.g.mcmillan@tudelft.nl

Dr. W. Egger
Institut für Angewandte Physik und Messtechnik
Universität der Bundeswehr München
Werner Heisenbergweg 39, D-85579 Neubiberg, Germany

Dr. M. Dickmann, Prof. C. Hugenschmidt
Physics Department and Heinz Maier-Leibnitz Zentrum (MLZ)
TU München
Lichtenbergstrasse 1, D-85748 Garching, Germany

**ADVANCED
SCIENCE NEWS**
www.advancedsciencenews.com

**ADVANCED
SUSTAINABLE
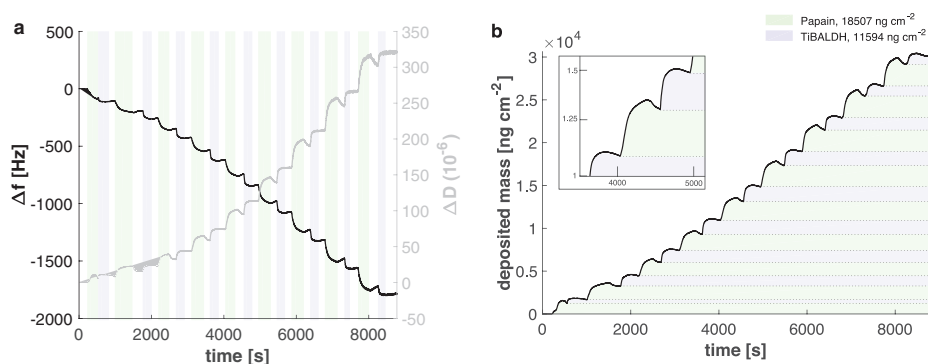SYSTEMS**
www.advsustainsys.com

nanoparticles of anatase-TiO$_2$[13] and quartz-like silicates under conditions that normally would not allow the formation of these crystalline products.[13,16] Unfortunately, studies in this area thus far appear to have had limited progress due to technical difficulties in protein handling. Fortunately, the enzyme chemistry of silicatein is highly related to that of other enzymes. One such enzyme is papain, which is cheaply produced, highly stable, and readily available. Recently, it was demonstrated that papain is capable of mineralizing titania when immersed in a lactate titania precursor solution.[16] This process showed the creation

Figure 1. a) QCM-D measurement of the deposition of a papain/titania 9-layer. Green regions indicate immersion using 1×10^{-3} M papain in 100×10^{-3} M MOPS pH 7.0, blue regions indicate immersion using 20×10^{-3} M TiBALDH, and the white regions stand for washes with distilled deionized water. b) Mass deposition extracted with QSense Dfind Composite Sauerbrey.[15]

of a layer containing anatase and rutile TiO$_2$ in addition to the formation of hydrolyzed lactate species as an organic fraction. However, several key questions in view of its application in energy materials were not yet addressed, such as the extent of multilayer stacking that may enable to tailor film thicknesses, and the potential of this method for the development of photovoltaic devices. Furthermore, the surface properties of the titania layer were not characterized and the quartz crystal microbalance with dissipation (QCM-D) modeling of the deposition did not yet take dissipation into account. To build upon these discoveries, in this study we demonstrate that the enzyme papain adsorbs on several oxide surfaces, including indium tin oxide (ITO), and forms thin layers covering the full area of the substrate, while it maintains its ability to catalyze the mineralization process of titania seemingly without limit. Such deposition of a sufficiently thick TiO$_2$ top layer opens up the possibility to create another papain layer on top of the previous papain/titania layer, enabling stacking of layers. These reactions were applied and integrated into a repeatable dip-coating procedure, resulting in a simple and flexible procedure to create hybrid enzyme/titania multilayer thin films. In addition, the synthesized films can be annealed at relatively low temperature for short duration to remove most of the organic material in the films and achieve a mesoporous titania thin film with a large surface area. Positron annihilation depth profiling revealed that the annealed papain/titania films contain less vacancy-related defects, indicating a higher quality titania. We demonstrate that the resulting nanoporous layer can be exploited to create a high surface area interface with an organic or inorganic photoactive dye layer for energy generation in DSSCs. These results suggest a new method to produce titania thin films with tunable thickness in low temperature, nonvacuum, nontoxic environments, and without the requirement for expensive technologies.

2. Results and Discussion
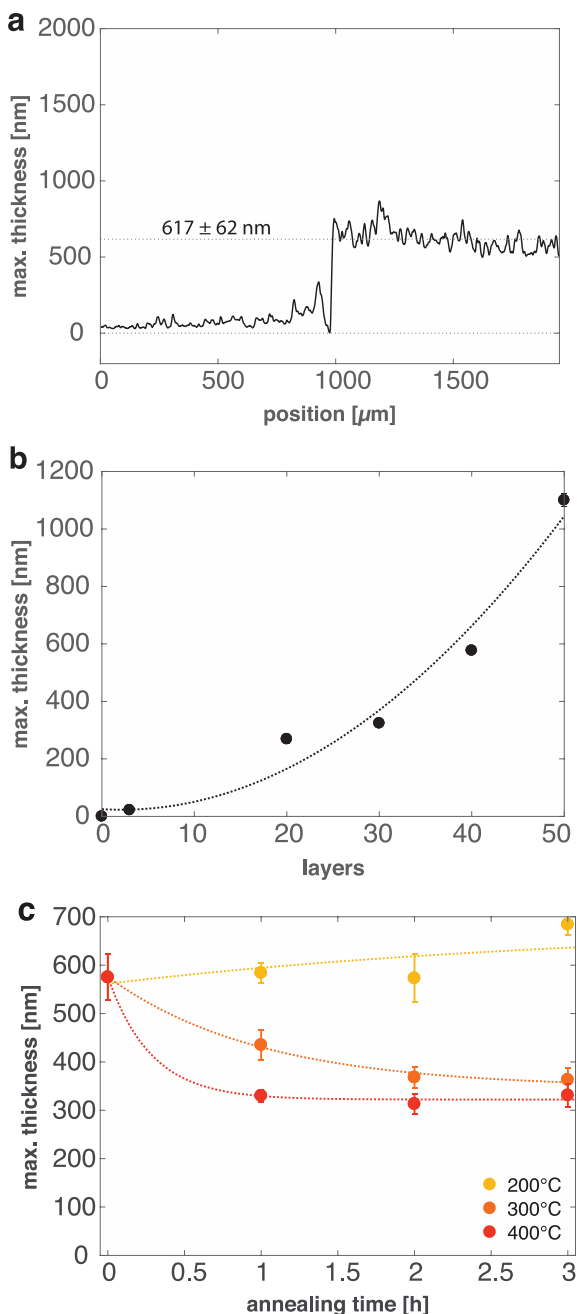
2.1. Synthesis and Characterization

In **Figure 1**a, the deposition of a stack of 9 papain/titania layers is shown as monitored by QCM-D. During immersion in the enzyme solution, the lowering in frequency (87 Hz) reflects growth of the adsorbed layer and the gain in dissipation (10×10^{-6}) reflects a decrease in stiffness of the adsorbed layer. These values are slightly higher compared to those observed during immersion in the titanium(IV) bis(ammonium lactato)dihydroxide (TiBALDH) solution (60 Hz, 5×10^{-6}). With increasing the number of stacked layers, the decrease in frequency is seen to enlarge by ≈13 Hz for papain immersions and by ≈3 Hz for TiBALDH immersions, while an additional increase in dissipation is observed of 5.5×10^{-6} for every papain immersion and of 1.5×10^{-6} for every TiBALDH immersion. The enzyme deposition exhibits biphasic behavior, with fast deposition during the first minute, after which a second phase with slower deposition follows. The water washes show that most of the material deposited in this second phase is washed off. Titania deposition consists of only one phase that is rapid at 0.54 µg cm^{-2} min^{-1} and saturates quickly. The dissipation measurements suggest that the enzyme layers are relatively soft whereas the titania layers behave as a rigid layer. The frequency differences were converted into deposited mass using the Composite Sauerbrey function[17] in QSense Dfind Software. Figure 1b shows that over 60% of the deposited mass is related to proteins in the papain solution. The maximum thickness of a 9-layer (nonalayer) assembly is typically around 600 ± 60 nm (**Figure 2**a). In profilometer measurements we refer to the thickness as maximum thickness, as the profilometer stylus, owing its relatively large tip diameter of 12.5 µm, slides over the highest peaks on the surface and therefore probes an average maximum thickness of the layer. Using this maximum thickness and the total mass deposited of 30 µg cm^{-2}, we can estimate a density of 0.49 g cm^{-3}, in agreement with Bawazer et al.[16] However, the deposited mass derived in this way is an underestimation due to viscoelastic effects in thick layers.[18,19] Analysis using the Kelvin–Voigt Model (Figure S3, Supporting Information), that takes these effects into account, leads to a larger deposited mass of 35 µg cm^{-2}, corresponding to a density of 0.58 g cm^{-3}. The densities of nanoparticulate TiO$_2$ and of papain typically are 4.2 and 1.2 g cm^{-3},[16,18,20] suggesting the papain/titania layer is not as dense as previously described,[16] but is actually highly porous.

Next, we sought to understand the limitations of layer-by-layer assembly and the kinetics involved. We were able to
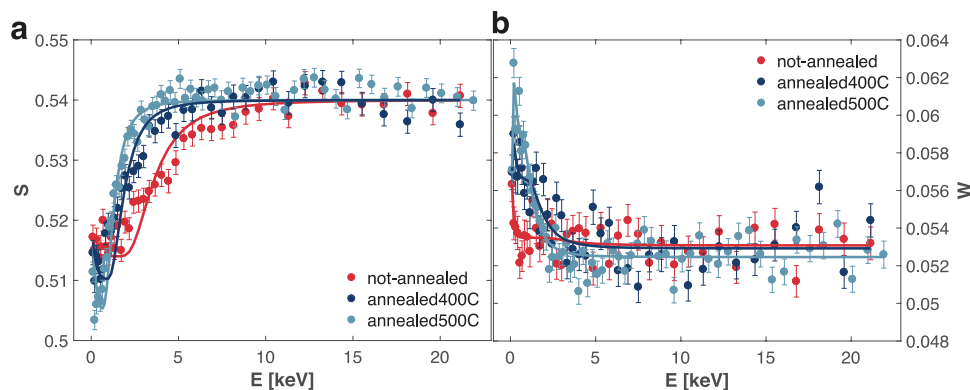
2000003 (2 of 12)

ADVANCED
SCIENCE NEWS
www.advancedsciencenews.com

ADVANCED
SUSTAINABLE
SYSTEMS
www.advsustainsys.com

Figure 2. a) Profilometry thickness measurement of as-deposited papain/titania nonalayer. b) Thickness of papain/titania layers as a function of number of deposited layers using 10×10^{-6} M papain in 20×10^{-3} M MOPS pH 7.0, determined from profilometry. c) Thickness of papain/titania nonalayers deduced from profilometry as a function of annealing time for three different annealing temperatures, 200, 300, and 400 °C.

repeatedly stack up to 50 layers (Figure 2b), with no limit to the layer-by-layer process indicated from these experiments. A triple layer produced using a concentration of 10×10^{-6} M shows a relatively small thickness of ≈20 nm (Figure 2b), but the growth rate increases substantially with the number of layers. At 35 layers the increase in thickness with each layer is ≈30 nm. The thickness of the as-deposited trilayers was

found to be larger (≈100 nm) for concentrations greater than 0.5×10^{-3} M, beyond which it remains independent of concentration (Figure S1, Supporting Information).

Annealing at temperatures of ≈300 °C and higher results in a marked decrease in thickness, that saturates at a decrease of ≈45% (Figure 2c). The decrease in thickness is caused by evaporation of organic remains in the layer and a subsequent compaction of the layer enabled by the high mobility of atoms in the titania layer during the annealing procedure.

Subsequently, we investigated the evolution of the layers by Doppler broadening positron annihilation spectroscopy (DB-PAS), in order to monitor the evolution of their thicknesses upon thermal annealing, and to examine the changes in composition and defects contained in the films. The Doppler broadening S parameter is a measure of positron annihilation with valence electrons, which provides sensitivity to the electronic structure and the presence of open volume defects such as vacancies or vacancy clusters.[21–23] The increase in concentration or size of vacancies or vacancy clusters in an otherwise identical material generally leads to an increase of the S parameter. The W parameter is a measure of annihilation with (semi-)core electrons which provides chemical sensitivity to the positron trapping site.[21–23] By tuning the positron implantation energy in the range of 0.1–25 keV, the subsurface regions of up to a few micrometers of the layered samples are probed as a function of average implantation depth $z_{ave} = \alpha_p E^n/\rho$ (in nanometers), with the positron implantation energy E in keV, the empirical value for the exponent set at $n = 1.62$, $\alpha_p = 4.0 \ \mu g \ cm^{-2} \ keV^{-1.62}$, and the density ρ in $g \ cm^{-3}$, assuming Makhovian positron implantation profiles.[22] The collected Doppler depth profiles (**Figure 3**) of papain/titania 9-layer (nonalayer) assemblies before and after thermal annealing were fitted using the VEPFIT program.[24] It can clearly be seen that the experimental and calculated S-parameter curves for the as-deposited nonalayer do not agree in the steepness of their slopes in the range of 2–8 keV in positron implantation energy, which are significantly less steep for the experimental curves than for the theoretical curves from the VEPFIT analysis that assumes a single thickness (i.e., a flat layer). This indicates a distribution in heights of the film in the measured area of ≈1 cm². Indeed, a simulation for an as-deposited papain/titania 50-layer (Figure S6, Supporting Information), based on a broad range of height distributions (ranging from 200 to 1100 nm), was found to provide a good agreement with the measured S-parameter depth profile. This affirms that the as-deposited films contain highly corrugated surfaces, not flat as previously proposed in Bawazer et al.[16] This was furthermore confirmed by scanning electron microscopy (SEM) imaging (**Figure 4**). In contrast to the profilometry measurements, the DB-PAS measurements that were fitted using a single layer model reflect the average thicknesses of the films. The best-fit parameters determined using VEPFIT (**Table 1**) reveal that the average thicknesses of the as-deposited and annealed nonalayers as probed by DB-PAS are indeed smaller than the maximum thicknesses determined by profilometry. Using the fit values for a nonannealed layer, we calculate a deposited mass of 27 $\mu g \ cm^{-2}$. This is somewhat lower than the Kelvin–Voigt-corrected deposited mass of 35 $\mu g \ cm^{-2}$ determined from the QCM-D measurements (Figure 1; Figure S3, Supporting Information). A reasonable

ADVANCED
SCIENCE NEWS

www.advancedsciencenews.com

ADVANCED
SUSTAINABLE
SYSTEMS

www.advsustainsys.com

Figure 3. Positron Doppler broadening. a) *S*-parameter and b) *W*-parameter depth profiles of papain/titania nonalayers before and after thermal annealing at 400 and 500 °C for 4 h. Dashed lines are fit curves to a single layer and substrate model obtained using VEPFIT analysis (see Table 1).

explanation for such a difference may be the presence of water contained within the nanoporous layers during the QCM-D measurements that are performed in water, leading to an overestimation of the mass contained in the nanoporous film (Figure S7, Supporting Information). Upon annealing at 400 °C, the average thickness decreases by more than 60%, indicating a loss of material from the film, similar to the results obtained by profilometry (Figure 2c). In addition, the *S*-parameter of the layer decreases while the *W*-parameter increases, suggesting a change in its composition. This feature is likely caused by evaporation of the organic remains from the film, and furthermore reflects a reduction in vacancy-related defects, as observed in the positron lifetime experiments that are discussed further on.

In order to gain further insights into the morphology of the films, SEM measurements of single papain/titania layers were performed (Figure 4). The SEM images show that as-deposited single papain/titania layers form fairly homogeneous films,

with a low density of particles with typical lateral dimensions of about 50–100 nm on top of the layer. After annealing, the single layer titania is transformed into a morphology with a smoother surface and visible pores, with diameters ranging from around 30–100 nm (Figure 4b). This is likely due to the combustion of protein from the layer during annealing, leaving behind empty spaces and holes in the layer. In parallel, the high atom mobility in the titania during annealing allows considerable local rearrangement of the titania around these empty spaces in the layer, resulting in the appearance of circularly shaped holes.

The papain/titania nonalayers were also studied using SEM and show a quite different morphology (Figure 4c,d). The as-deposited layers are characterized by highly corrugated films, containing many hills and valleys at large height differences, in line with the positron DB-PAS results that represent an average over a much larger area of ≈1 cm². After annealing the surface of the nonalayer appears to be flattened out, but still exhibits clear differences in height. The annealed film contains irregular cracks, likely caused by the same phenomenon occurring in the single layer deposition, related to evaporation of the organic remains, indicating that here all layers are connected by open porosity.

In view of solar cell applications, we investigated in addition the deposition of papain/titania layers on ITO-coated glass substrates and their evolution into a titania layer upon subsequent thermal annealing. ITO/TiO₂ layer architectures are commonly applied in state-of-the-art solar cells based on, e.g., perovskite absorber layers and dye sensitizer layers.[5] The high conductivity of the ITO layer is also beneficial as it prevents charging of samples during SEM imaging. Indeed, deposition of the papain/titania layers on ITO-coated glass substrates allowed us to obtain SEM images at higher resolution, and the thickness of layers could be determined by cross-sectional SEM measurements (**Figure 5**; Figure S9, Supporting Information). The deposited single papain/titania layer annealed at 450 °C for 4 h shows
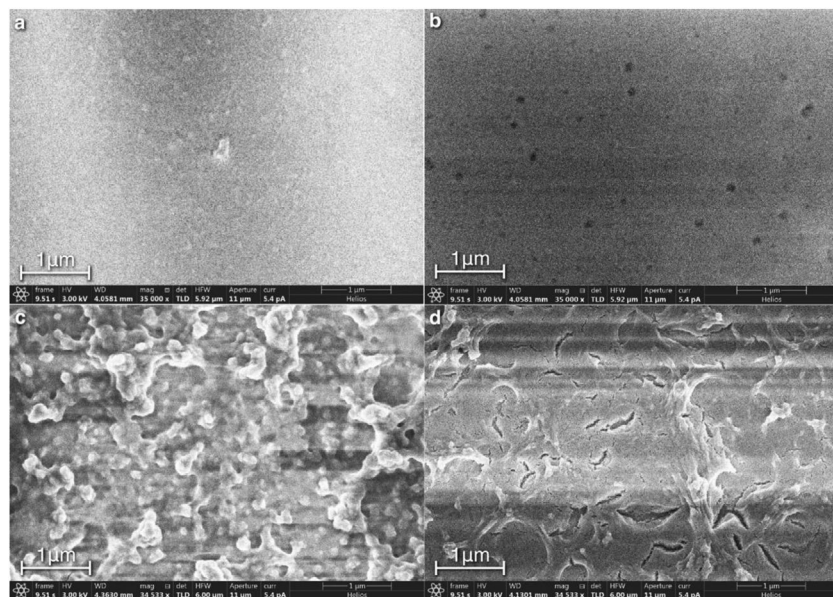
Figure 4. SEM images of a) a single papain/titania layer, b) an annealed papain/titania layer, c) a papain/titania 9-layer, and d) an annealed papain/titania 9-layer, at 35 000× magnification. Annealing was done at 400 °C for 4 h.

ADVANCED
SCIENCE NEWS
www.advancedsciencenews.com

ADVANCED
SUSTAINABLE
SYSTEMS
www.advsustainsys.com

Table 1. Papain/titania (PT) nonalayers: VEPFIT parameters, with d the thickness, S- and W-parameter, L_+ the effective positron diffusion length, and ρ the density.

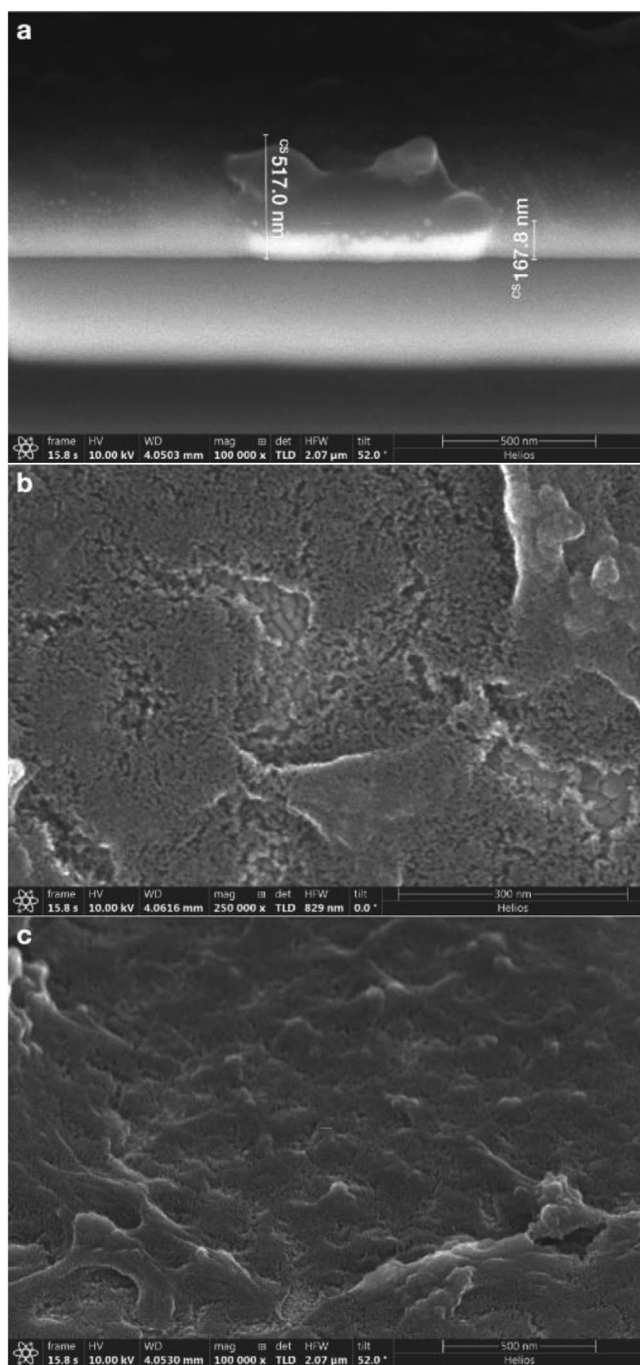|	d	S	W	L_+	ρ
PT (not-annealed)[a]	463 nm	0.514 ± 0.001	0.0535 ± 0.0005	7 nm	0.59 g cm^{-3}
PT (400 °C)[a),b]	150 nm	0.510 ± 0.001	0.0565 ± 0.0005	7 nm	0.64 g cm^{-3}
PT (500 °C)[a),b]	80 nm	0.504 ± 0.001	0.0586 ± 0.0005	7 nm	0.64 g cm^{-3}
SiO$_2$	semi-infinite	0.540 ± 0.001	0.0532 ± 0.0005	5 nm	2.33 g cm^{-3}
SiO$_2$ (400 °C)	semi-infinite	0.540 ± 0.001	0.0529 ± 0.0005	5 nm	2.33 g cm^{-3}
SiO$_2$ (500 °C)	semi-infinite	0.540 ± 0.001	0.0525 ± 0.0005	5 nm	2.33 g cm^{-3}

[a]1×10^{-3} M papain in 100×10^{-3} M MOPS pH 7.0 is used; [b]Annealing was carried out for 4 h.

a thickness of 37 nm, while the ITO coating layer underneath is much thicker, around 340 nm (Figure S9, Supporting Information). The surface of the papain/titania layer (Figure S10, Supporting Information) contains grains with lateral dimensions in the range of 20–30 nm which are typical for the grains in ITO coatings,[25,26] demonstrating that the single papain/titania layer closely follows the morphology of the ITO coating. Like for the case of papain/titania layers on bare glass substrates, the annealing of layers on ITO also leads to the creation of holes in the papain/titania. SEM images of a papain/titania nonalayer deposited on ITO-coated glass (Figure 5) reveal that, in contrast to the single layer, the nonalayer exhibits a variation in thickness. The cross-sectional SEM image shows a minimum thickness of the layer of ≈170 nm. The large extrusion on top results in a maximum thickness of around 500 nm, corresponding well with the thickness determined by profilometry. This may in a direct manner account for the large differences in measured thicknesses obtained from the positron DB-PAS (**Table 2**), reflecting the average thickness of around 225 nm, and profilometry (Figure 2), reflecting the maximum thickness of the layer. It is noteworthy that in annealed samples the papain/titania is absent in some areas, as visible in Figure 5b that shows the presence of cracks in the layer, exposing the characteristic morphology of the ITO coating underneath. The tilted image in Figure 5c clearly shows a marked distribution in heights of the film and the ITO coating that is visible through the cracks in the layer after thermal annealing. Energy dispersive X-ray spectroscopy (EDX) measurements on the annealed papain/titania nonalayer (Figure S11, Supporting Information) showed contributions of the titania and ITO layers, the glass substrate and organic remains in the film. The titania films exhibit amorphous features in X-ray diffraction (Figure S12, Supporting Information), suggesting that the films are either amorphous, or consist of nanoparticles or very small domains, as previously observed.[16]

In order to compare with the deposition on bare glass surfaces, enzymatically synthesized titania layers deposited on ITO-coated glass substrates were analyzed using positron DB-PAS depth-profiling and positron annihilation lifetime spectroscopy (PALS). In **Figure 6**, the Doppler S and W parameter depth profiles of a nonalayer on ITO, annealed at 400 °C, are compared to the depth profiles of 1) a bare annealed ITO-coated glass substrate and 2) a reference sample consisting of TiO$_2$, produced using electron beam physical vapor deposition (EBPVD), on ITO-coated glass, denoted here as the EBPVD

TiO$_2$-ITO reference sample. The S and W plateaus corresponding to the EBPVD TiO$_2$ layer are clearly visible for the TiO$_2$-ITO reference sample in the range of positron implantation energies up to 2 keV. The Doppler depth profiles for the annealed papain/titania nonalayer indicate the presence of a small plateau at implantation energies of around 1 keV. In Table 2, the parameters of the papain/titania, ITO, and glass layers of the nonalayer sample are displayed, extracted from VEPFIT-analysis using a two-layer model with a semi-infinite substrate. The S and W parameters of the ITO and glass were fixed at the values deduced from the measurements on the annealed ITO reference sample (ITO-a). The extracted average thickness of 225 nm of the papain/titania nonalayer is reasonable considering the typical thicknesses and morphology of the corrugated papain/titania layer deduced from the SEM image of Figure 5a. Notably, the annealed nonalayer has a slightly lower S-parameter value ($\Delta S/S_0 \approx -3\%$) and a significantly higher W-parameter value ($\Delta W/W_0 \approx +18\%$) than the S,W values obtained for EBPVD TiO$_2$, pointing to a reduction in vacancies induced by the annealing. We note that, due to the corrugated nature of the papain/titania layer, also annihilation of positrons at the surface and in the ITO layer may have some (minor) effect on the extracted S and W parameter of the relatively low-density porous thin papain/titania layer.

In order to gain quantitative insights into the differences in vacancies and in porosity of the papain/titania nonalayers before and after annealing, PALS measurements were performed. Namely, the positron lifetime of positron annihilation in vacancies or vacancy clusters in a given material is a measure of their size. Moreover, PALS has a proven high sensitivity to determine vacancy concentrations in the range of about 10^{-6}–10^{-3} atomic fraction.[21,27] Representative spectra collected for the as-deposited and annealed nonalayers at a positron implantation energy of 0.5 keV are shown in **Figure 7**a, in comparison with the PALS spectrum obtained for the EBPVD TiO$_2$ reference sample. This low energy corresponds to a mean positron implantation depth of ≈3 nm in dense TiO$_2$ (≈4.2 g cm^{-2}) and of ≈10 nm in a dense papain layer (≈1.2 g cm^{-2}),[16] indicating that the surface and the region just below the surface of the layers is probed. Figure 7a shows that the EBPVD TiO$_2$ layer exhibits the strongest long lifetime component, that is largely reduced in intensity at 1.0 keV (Figure S13, Supporting Information), indicating ortho-Positronium (o-Ps) is formed at the surface of the TiO$_2$ layer that annihilates subsequently via pick-off annihilation. In contrast, the o-Ps pick-off component for the

**ADVANCED
SCIENCE NEWS**

www.advancedsciencenews.com

**ADVANCED
SUSTAINABLE
SYSTEMS**

www.advsustainsys.com

Figure 5. a) Cross-section of annealed papain/titania nonalayer deposited on ITO-coated glass showing a minimum thickness of ≈170 nm and a maximum thickness of ≈520 nm. b) Surface of the annealed nonalayer on ITO-coated glass. c) Tilted image of the annealed nonalayer exposing the ITO-layer underneath the papain/titania layer and showing the differences in heights of the PT-film.

nonalayers does not diminish strongly with positron implantation energy, indicating the presence of nanopores inside the papain/titania nonalayers. Intriguingly, the annealed papain/titania layers show a longer o-Ps pick-off lifetime component than the nonannealed nonalayers, but with lower intensity, suggesting a decrease in the amount of nanopores upon thermal

annealing, while their pore sizes grow. Furthermore, Figure 7a shows that the short lifetime component of the annealed layer is shorter than for both the as-deposited nonalayer and the EBPVD TiO_2 layer, indicating that annealing leads to a reduced concentration of vacancies or size of small vacancy clusters, in line with the 3% reduction in S parameter and the 18% large increase in W parameter observed by DB-PAS, and the strong reduction in the average positron lifetime in the range of 1–2 keV positron implantation energy (Figure 7b).

These conclusions are supported by a full, quantitative four-lifetime-component analysis of the lifetime spectra using the POSWIN program package.[28,29] A four-component analysis was required for all samples in order to achieve satisfactory fits. **Figure 8** provides an overview of the best-fit analysis of the PALS spectra of the as-deposited and the annealed papain/titania nonalayers, the EBPVD TiO_2 reference sample and the ITO-layer on glass sample at 1 keV. The annealing of the papain/titania nonalayer induces a marked reduction in average positron lifetime at a positron implantation energy of around 1 keV (Figure 7b), where the nonalayer is optimally probed (as can also be inferred from the Doppler depth profiles of Figures 3 and 6). The Doppler depth profiles indicate that the reference EBPVD TiO_2 layer is also probed optimally at 1 keV, while the ITO layer of the ITO-coated glass reference is best probed at 2 keV. **Table 3** presents the corresponding positron annihilation lifetime parameters extracted from the four-component analysis.

The EBPVD TiO_2 layer exhibits a dominant 399 ps component and a minor 130 ps short component. Ab-initio calculations indicate that the positron lifetime of defect-free rutile TiO_2 is ≈151–158 ps,[30,31] that is close to the experimental value of 155–157 ps,[30,32] while the calculated positron lifetime of defect-free anatase TiO_2 is longer, ≈184 ps,[31] in line with the experimental lifetime of ≈178 ps.[33] Comparison to previous studies that report significant contributions of positron annihilation with a lifetime in the range of 360–390 ps[33,34] indicate that the EBPVD TiO_2 layer contains abundant vacancy clusters with a size at least equal to, but likely larger than, a V_{Ti}-V_O divacancy. In TiO_2 powders, lifetimes in the range of ≈370–440 ps were attributed to surface annihilation.[35,36] The observed 130 ps component may correspond to the reduced bulk lifetime encountered in a two-state trapping model.[21] The ITO layer, in contrast, shows two short lifetime components at 188 and 371 ps of equal intensity, resulting in an average short lifetime of $<\tau_s> ≈ 275$ ps, defined as $<\tau_s> = (I_1\tau_1 + I_2\tau_2)/(I_1 + I_2)$, that is much shorter than $<\tau_s> ≈ 377$ ps of EBPVD TiO_2.

The as-deposited papain/titania nonalayer shows a dominant short lifetime component of 373 ps besides a minor short lifetime component of 79 ps. Remarkably, as Table 3 shows, both the lifetimes and intensities of these two shortest lifetime components are close to those of the EBPVD TiO_2 layer, in line with the close similarity of the PALS spectra of the two layers at 1 keV (see Figure 8a,c). We furthermore note that the S- and W-parameter of as-deposited papain/titania nonalayer are also close to those of EBPVD TiO_2 (see Tables 1 and 2), suggesting that the dense titania in the as-deposited nonalayer contributes most strongly to the positron annihilation at 1 keV, and exhibits similar characteristics as EBPVD TiO_2. Upon thermal annealing of the papain/titania nonalayer, the intensity of the

ADVANCED
SCIENCE NEWS
www.advancedsciencenews.com

ADVANCED
SUSTAINABLE
SYSTEMS
www.advsustainsys.com

Table 2. VEPFIT parameters of layers on ITO-coated glass substrates with d the thickness, S- and W-parameter, L_+ the effective positron diffusion length, and ρ the density.

|	d	S	W	$L+$	ρ
ITO (annealed)[b]	70 nm	0.476 ± 0.001	0.0760 ± 0.0005	5 nm	7.14 g cm^{-3}
PT nonalayer[a] (annealed)[b] on ITO	225 nm	0.500 ± 0.001	0.0623 ± 0.0005	5 nm	0.64 g cm^{-3}
TiO$_2$	50 nm	0.516 ± 0.001	0.0530 ± 0.0005	7 nm	4.20 g cm^{-3}
SiO$_2$	semi-infinite	0.540 ± 0.001	0.0530 ± 0.0005	3 nm	2.33 g cm^{-3}

[a]1×10^{-3} M papain in 100×10^{-3} M MOPS pH 7.0 is used; [b]Annealing was carried out at 400 °C for 4 h.

dominant component of 382 ps characteristic of vacancy clusters reduces to 58%, while a fairly strong 209 ps lifetime component emerges. This lifetime is somewhat larger than that of defect-free TiO$_2$, indicating a contribution of Ti monovacancies, while on the other hand it is slightly shorter that the lifetime of 230–260 ps observed for amorphous TiO$_2$ nanoparticles,[36] and much shorter than the lifetime characteristic for vacancy clusters. This reveals a reduction in concentration and/or size of the vacancy-related defects in the titania upon thermal annealing, supported also by the strong reduction in the average positron lifetime compared to the as-deposited papain/titania nonalayer (Figure 7b) and EBPVD TiO$_2$ (Figure S14, Supporting Information). This could be expected, since the mobility of atomic species in titania is large at the annealing temperature of 400 °C, leading to restructuring of the titania. The observed second lifetime component for the 9PTa sample at 382 ps is strongest at 1 keV, where the papain/titania layer is probed (Table 3), correlating with the dominant contribution of annihilation in the annealed papain/titania layer at 1 keV. This suggests that the titania still contains some vacancy clusters, or that some of the positrons annihilate at the surfaces of the nanoporous titania layer. In conclusion, the PALS study shows that annealing of the papain/titania layers causes a reduction in the concentration and/or size of small vacancy-clusters, while annihilation in vacancy clusters or surface annihilation is also observed.

Furthermore, the four-component fits reveal the presence of two additional, long lifetime components for the nonalayers, the first one with a lifetime of around 1.3–2 ns and intensity of 2.5% for the as-deposited papain/titania nonalayer, pointing to o-Ps

pick-off annihilation in small micropores, with a size of around 0.5–0.7 nm in diameter according to the Tao–Eldrup model.[37–39] Besides, a second long lifetime component with a positron lifetime of ≈3.7 ns is seen, indicating the presence of micropores with a diameter of around 0.9 nm. Interestingly, upon annealing, the small micropores disappear while the intensity of the larger micropores remains nearly the same. In parallel, the background of the PALS spectrum increases, indicating the formation of larger nanopores, open porosity or surface formation of Ps that is emitted into the vacuum. This indicates that the small micropores anneal or cluster into larger nanopores. Also, some of the positronium formed in the as-deposited papain/titania nonalayer could arise from open volume in the papain, that is effectively removed upon thermal annealing at 400 °C for 4 h.

Indeed, the presence of larger pores for annealed papain/titania multilayers was revealed by 3γ-annihilation of o-Ps observed in the energy spectra of the annihilation gamma-ray photons collected during the DB-PAS experiments (Figure S17, Supporting Information). Detection of 3γ-annihilation requires the presence of an appreciable amount of sufficiently large nanopores, typically a fraction of closed porosity in the layer above ≈10%, consisting of nanopores with a size of the order of ≈20 nm at least, or open porosity that offers the possibility for o-Ps escaping into the outer vacuum. Clearly, the annealing induces the appearance of 3γ-annihilation in the range of positron implantation energies between 1 and 3 keV, indicating the formation of large nanopores and/or open porosity in the papain/titania nonalayer. The latter may reflect the higher surface area due to the highly corrugated surface of the annealed papain/titania observed by SEM, offering
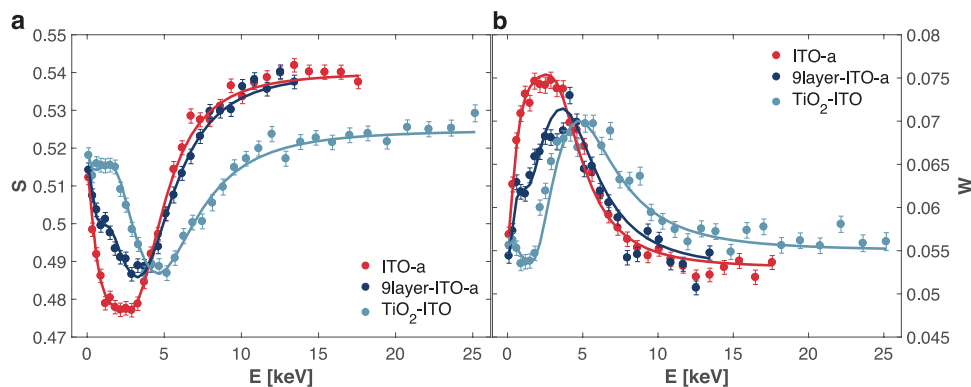
Figure 6. Comparison of DB-PAS depth profiles of papain/titania nonalayer on ITO-coated glass and the EBPVD-TiO$_2$ and annealed ITO reference samples. Dashed lines are best-fits from VEPFIT analysis (see Table 2). The reference sample is made with electron-beam physical vapor deposition and has a thicker ITO coating of ≈100 nm, and a different type of glass substrate. Annealing of the nonalayer and of the ITO reference sample is done at 400 °C for 4 h.
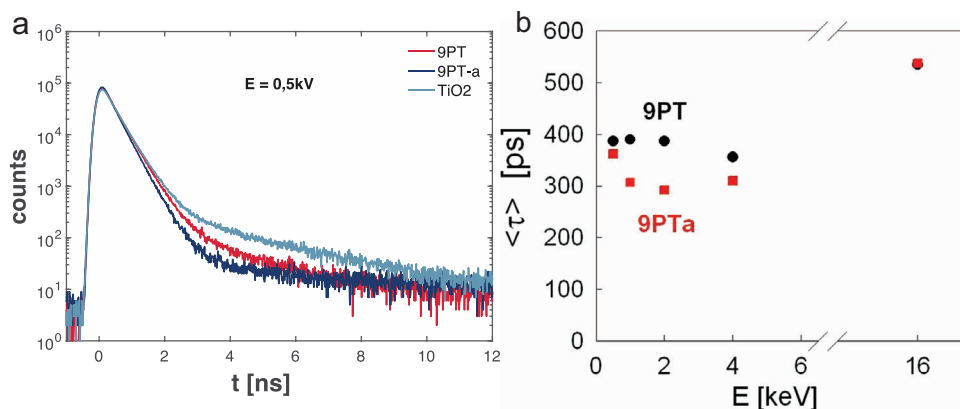
Figure 7. a) Positron annihilation lifetime spectra of as-deposited and annealed (450 °C, 4 h) papain/titania nonalayers and EBPVD TiO$_2$ for an implantation energy of 0.5 keV. b) Average positron annihilation lifetime <τ> as a function of positron implantation energy from a 4-component lifetime analysis of a papain/titania nonalayer (9PT) on ITO-coated glass before and after thermal annealing at 400 °C for 4 h.

abundant surface sites where the positron can pick up an electron to form o-Ps and escape into the open space. The appearance of 3γ-annihilation demonstrates that annealing not only leads to a reduction in vacancy-related defects in the titania and a corresponding higher quality of the layer, but also induces the creation of favorable open mesoporosity of the titania layer, that offers opportunities for applications in solar cells where a large interface area between the titania electron transport layer and the solar cell absorber layer is highly desirable.

2.2. Application

The papain/titania films were successfully applied in a first construction of a DSSC in which enzymatically synthesized papain/titania layers are combined with a natural dye and a water-based electrolyte solution, as schematically represented in **Figure 9**. A photovoltage is directly observed upon exposure of this first set of test devices to ambient daylight. The photovoltage increases with thickness of the stacked papain/titania multilayers. Three-to-fifteen layer stacks of annealed papain/titania layers show increasingly higher open circuit voltage of $V_{oc,3}$ = 3.2 mV, $V_{oc,9}$ = 13.1 mV, and $V_{oc,15}$ = 35.0 mV, respectively, at similar illumination conditions, see Figure 9. This is an encouraging result in view of future applications in DSSCs. For these first test devices, the observed closed circuit current density J_{SC} was nevertheless still very low, in the order of μA cm^{-2} only, showing that further research is needed to further develop and optimize implementation of these layers in photovoltaic devices to produce high-efficiency DSSC solar
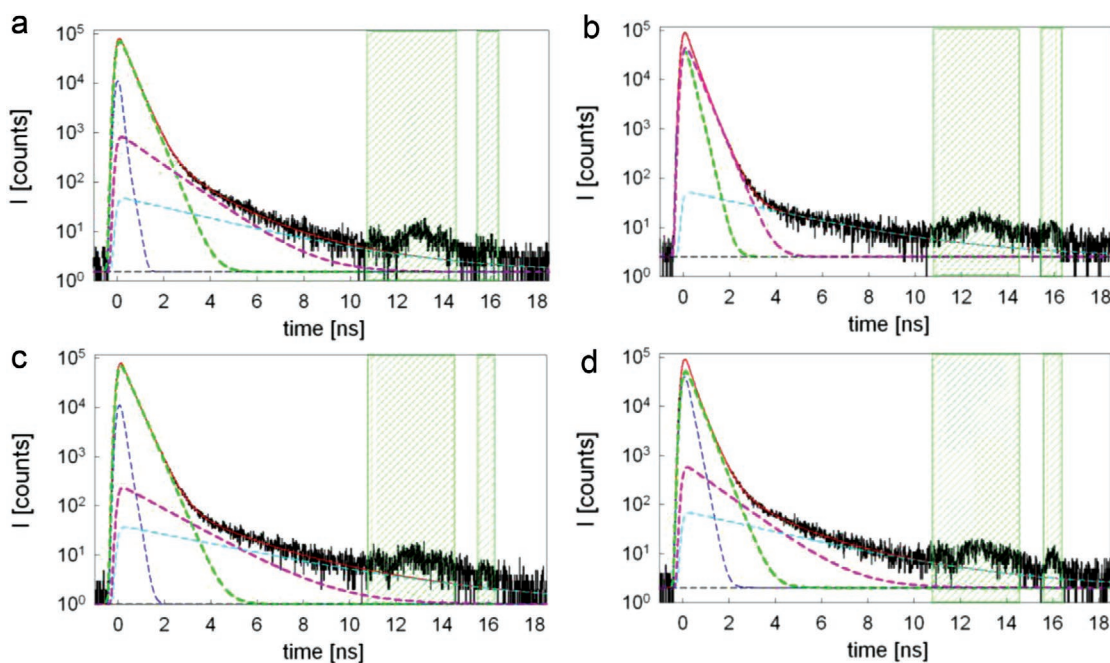
Figure 8. PALS spectra at 1 keV and fits obtained using POSWIN of a) papain/titania nonalayer, b) annealed (450 °C, 4 h) papain/titania nonalayer, c) TiO$_2$ reference sample fabricated using EBPVD, and d) ITO layer on glass substrate. The regions between 10.8 and 14.5 ns as well as 15.6–16.2 ns have been excluded from fitting, due to the presence of spurious peaks of annihilation by backscattered positrons.

Table 3. Positron lifetimes and intensities for the papain/titania nonalayer (9PT), the papain/titania nonalayer after annealing (9PTa), and the EBPVD TiO$_2$ on ITO-coated glass substrates, at a positron implantation energy of 1 keV, extracted from a four-lifetime component analysis of the PALS spectra in the time range up to $t = 33$ ns after positron implantation using the POSWIN program.

	τ_1 [ps]	τ_2 [ps]	τ_3	τ_4 [ns]	I_1 [%]	I_2 [%]	I_3 [%]	I_4 [%]	I_{bg} [counts]
9PT (1 keV)	79 ± 4	373 ± 1	1.3 ± 0.1 ns	3.7 ± 0.3	7.1 ± 0.2	89.9 ± 0.2	2.7 ± 0.1	0.31 ± 0.01	1.5
9PTa (1 keV)[a]	(5 ± 3)[a]	209 ± 5	382 ± 3 ps	3.8 ± 0.1	7.8 ± 0.6	34 ± 2	58 ± 2	0.41 ± 0.01	2.5
TiO$_2$ (1 keV)	130 ± 5	399 ± 1	1.7 ± 0.1 ns	4.5 ± 0.3	8.3 ± 0.4	90.5 ± 0.5	0.9 ± 0.1	0.35 ± 0.06	1.0
ITO (2 keV)	188 ± 3	371 ± 5	1.1 ± 0.1 ns	5.8 ± 0.6	48 ± 2	50 ± 2	1.6 ± 0.2	0.09 ± 0.01	1.3

[a]Note: The first component in this particular fit cannot be resolved given the instrument time resolution function, and is therefore also not plotted in Figure 8b.

cells. Many other photosensitive (natural) dyes could be used in combination with the papain/titania layer as long as they have an anchoring group that allows adsorption on titania, in order to facilitate the formation of a monolayer on its surface. Natural dyes usually have narrow absorbance peaks in the range of 300–600 nm, and record DSSC efficiencies of up to 1.7%,[40,41] while synthetic dyes can have broader peaks in a wider range from 200 to 800 nm and currently much higher record DSSC efficiencies of 12–13%,[5,42] with reported open circuit voltage V_{OC} of 0.91 V, short circuit current density J_{SC} of 18.1 mA cm^{-2} and fill factor (FF) of 0.78 for (expensive) ruthenium organometallic complexes.[43] This indicates that a search for natural dyes with significant absorbance in the near infrared or UV optical range is important for progress in the development of sustainable DSSCs. Natural dyes are important alternatives to synthetic dyes such as ruthenium organometallic complexes, due to their much lower cost, ease of fabrication, abundancy and sustainability.[40,41] Furthermore, an important future research topic will be the creation of an intimate TiO$_2$ photoanode/water-based electrolyte interface and the tailoring of its hydrophilicity,[43] as one of the key issues in order to progress toward optimized, high efficiency devices based on our
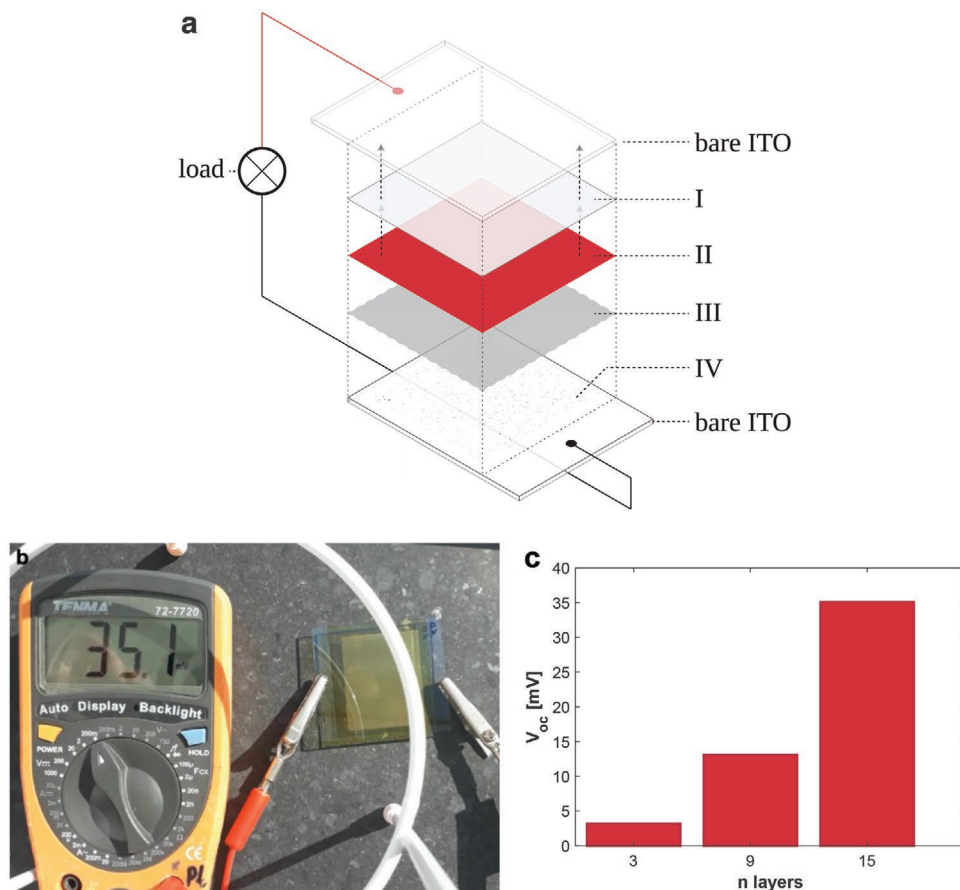
Figure 9. a) Exploded view of different layers of the dye-sensitized solar cell (DSSC) test devices. I) ITO–glass with ITO-coating facing inward, II) the deposited annealed papain/titania layer, III) adhered dye-layer from pomegranate juice, IV) liquid electrolyte (I$^-$,I$_3^-$) Lugols solution 5%, and V) graphite layer from pencil. The positive and negative contact have been indicated by the red and black line, respectively. b,c) Maximum determined open circuit voltage V_{oc} of the DSSCs with different stacks of annealed papain/titania layers. Voltages were measured with a multimeter.

**ADVANCED
SCIENCE NEWS**
www.advancedsciencenews.com

**ADVANCED
SUSTAINABLE
SYSTEMS**
www.advsustainsys.com

synthesis method. Our innovative synthesis of DSSCs based on enzymatically produced TiO_2 photoanodes combines a natural dye with the use of (sustainable) aqueous electrolytes, that witnessed increasingly intensive research efforts during the last decade, with highly promising results in terms of efficiency and stability.[43]

The enzymatically produced titania layers may furthermore find application in a wide range of other products that contain titania thin films as a functional layer, as it offers a highly flexible, accessible, and low-cost methodology to create titania thin films. This new fabrication technique also allows for tunability of titania film thicknesses, production of layers with mixed-cation oxide compositions (such as Ti-Mg oxides) and a great flexibility to create alternating cation oxide layers simply by selecting appropriate dip-coating sequences.

3. Conclusion

The enzyme papain was used successfully in a room temperature dip-coating procedure to synthesize multilayered porous titania/papain thin films, providing a straightforward, low-cost, and ecological method to produce titania thin films with tunable thickness. QCM-D measurements showed that the dip-coating process is simple and reliably reproducible, allowing the stacking of layers, with a stack of up to 50 layers being achieved with no indication of an upper limit in the amount of layers that can be stacked. Annealing at 400 °C for 4 h results in the evaporation of the organic remains in the film and produces a thinner, more solidified, porous and purer titania layer, that contains smaller or less vacancy-related defects than as-deposited material as indicated by the positron annihilation studies. As previously observed, as-deposited titania films are either amorphous, consist of nanoparticles, or consist of very small crystalline domains. SEM images in combination with profilometry and positron Doppler depth profile measurements showed that the layers have a corrugated surface and a large variation in local thickness of the films, whereas after annealing the films exhibit a unique cheese-like resemblance containing holes with diameters of 20–170 nm, depending on the annealing time and temperature, showing high tunability in morphology. After thermal annealing that leads to evaporation of the proteins, the density of the papain/titania layers still remains relatively low at $\rho \approx 0.6$–0.7 g cm^{-3}, indicating that the films have a high degree of porosity. Indeed, PALS shows that the as-deposited layers contain micropores with a diameter of ≈ 1 nm, and smaller micropores with $d \approx 0.5$–0.7 nm that largely disappear upon annealing. PALS and positron 3γ-annihilation measurements indicate that the thermal annealing induces the appearance of very large nanopores and/or open porosity. The creation of such mesoporous titania layers with highly corrugated surfaces offers opportunities for application in DSSC, where high interface area between the titania electron transport layer and the solar cell absorber layer is highly desirable.

In order to provide a first indication of its applicability, we combined the enzymatically synthesized annealed titania-layers with a natural dye and a water based electrolyte solution to build a very accessible, sustainable and low-cost solar cell, both from the fabrication and components' perspectives. The

method allows for tunability of titania film thicknesses and a great flexibility to create alternating layers simply by selecting appropriate dip-coating sequences, and it can be used to create layers with a high degree of nanoporosity. The environmentally friendly, low-cost method to create titania thin films offers good perspectives for application in dye-sensitized and perovskite solar cells, and may furthermore find application in many other products that contain titania functional layers.

4. Experimental Section

Preparation of Glass Slides/QCM-D Quartz Chips: The glass slide/QCM-D quartz chip samples were immersed in distilled water with 0.05% SDS detergent and sonicated for 10 min 3 times, followed by sonication in distilled water 5 times. In a fume hood, 5 g KOH was dissolved in 100 mL ethanol. Then the samples were again sonicated for 10 min in this solution. The last step consists of sonicating the samples three times in distilled deionized water while refreshing the water between each sonication step.

Preparation of Dip-Coating Procedure: To create an enzyme solution, the papain powder from Papaya latex (4.7 g) was dissolved in 200 mL, 100×10^{-3} M 3-(N-morpholino)propanesulfonic acid (MOPS, pH 7.0). To create the TiBALDH solution, TiBALDH (50% wt, 2 mL) was added to distilled deionized water (200 mL). This solution was stirred such that all the lactate was distributed evenly in the solution.

Dip-Coating Procedure: A glass substrate or ITO-coated glass substrate was inserted in the papain solution using tweezers or a scoop, where it was left for 5 min. Then, the remaining liquid was removed from the sample by shaking before putting the sample in the first beaker with distilled deionized water. There it remained for 30 s while slowly stirring. After thirty seconds, the sample was put into the TiBALDH solution for 2 min. Finally, the sample was put into the second beaker with distilled deionized water for thirty seconds, while slowly stirring. This procedure can be iterated as many times as desired to produce multilayered films. When finished, the samples were dried with nitrogen gas. Note: During some of these dip-coating processes, the papain solution was seen to become cloudy after more than seven iterations, caused by remains of the TiBALDH solution that mix with the papain solution, leading to enzymatic reactions that create TiO_2 in solution. This type of contamination of the solution can be spotted earliest in the papain solution but may happen in all solutions. Every ten cycles, the solutions were refreshed.

Thermal Annealing: A ceramic plate or bowl was used as a container for the samples during the annealing. The samples were heated in a calcination oven in 1 h from room temperature to the preselected thermal annealing temperature in the range of 200–500 °C, and kept at this temperature for 4 h, after which the oven cooled down to room temperature in 6 h.

Fabrication of Organic Dye Sensitized Solar Cell: The dye was extracted from pomegranates, which were cut and squeezed in a large beaker. A cloudy juice was extracted by sifting, and was subsequently filtered to achieve a clear purple pomegranate juice. Titania films were immersed for 24 h in the pomegranate juice to enable adhesion of the dye molecules. The immersion was carried out at room temperature in low-light conditions to prevent destabilization of the dye. Afterward the dye-coated slide was rinsed with ethanol and dried with nitrogen gas to ensure that no water was left in the film.

ITO-coated glass was used as a substrate to deposit the papain/titania layers. On one side, 1 cm was taped off to prevent deposition of a layer, such that this side can be used for electrical connection to the ITO coating. The substrate was subsequently annealed following the procedure described above, after which the annealed film was immersed in filtered pomegranate juice for 24 h. The other slide was coated with a small amount of graphite from a pencil by coloring the glass. Again, 1 cm was taped off to enable the second electrical connection, to the graphite coating. A small drop of Lugols Solution 5% (1 M KI and 0.1 M I_2)

in water was subsequently put on the slide with the titania layer. The slide with the graphite was put on top of the titania-coated slide, with the graphite counter electrode facing the dye-sensitized titania layer. The two slides were pressed together to let the electrolyte spread out and were fixed together using clamps. Subsequently, a multimeter can be connected for the *I–V* measurements (Figure 9).

Materials: Papain fruit extract in powder form was purchased from Shaanxi Sangherb Bio-Tech Inc. (CAS: 9001-73-4) and used in all experiments unless stated otherwise. TiBALDH (Sigma Aldrich, CAS: 65104-06-5), and Mg-Lactate (Sigma Aldrich, CAS: 1220086-24-7) was used.

Instrumentation: DB-PAS and 3γ-factor measurements were carried out with the variable energy positron beam (VEP) situated at the Reactor Institute Delft. The S- and W-parameter depth profiles were fitted using VEPFIT.[22]

Positron annihilation lifetime spectroscopy (PALS) experiments were carried out using the PLEPS spectrometer[44] of the NEPOMUC facility[45] which was situated at the Heinz Maier-Leibnitz Zentrum (MLZ) research reactor FRM II, Technische Universität München, Garching. All spectra were decomposed by four-component positron lifetime analysis in the time range of up to 33 ns after positron implantation using the POSWIN program.[28,29]

A QSense Analyzer and AT-cut quartz discs were used for the QCM-D measurements. The data were analyzed with the QSense software.

A Dektak 8 profilometer (Veeco/Bruker) was used to measure the thickness of the films.

An X'pert PRO Philips/PANalytical X-ray diffractometer was used to carry out the XRD measurements. The SEM images and the EDX experiments have been carried out using a FEI Helios G4 CX Scanning Electron Microscope.

Supporting Information

Supporting Information is available from the Wiley Online Library or from the author.

Conflict of Interest

The authors declare no conflict of interest.

[1] M. Grätzel, *Acc. Chem. Res.* **2009**, *42*, 1788.
[2] T. P. Chou, C. Chandrasekaran, S. J. Limmer, S. Seraji, Y. Wu, M. J. Forbess, C. Nguyen, G. Z. Cao, *J. Non-Cryst. Solids* **2001**, *290*, 153.
[3] P. T. Hammond, *Adv. Mater.* **2004**, *16*, 1271.
[4] P. Löbl, M. Huppertz, D. Mergel, *Thin Solid Films* **1994**, *251*, 72.
[5] A. Polman, M. Knight, E. C. Garnett, B. Ehrler, W. C. Sinke, *Science* **2016**, *352*, aad4424.
[6] H. Si, Z. Kang, Q. Liao, Z. Zhang, X. Zhang, L. Wang, Y. Zhang, *Sci. China Mater.* **2017**, *60*, 793.
[7] K. M. Roth, Y. Zhou, W. Yang, D. E. Morse, *J. Am. Chem. Soc.* **2005**, *127*, 325.
[8] M. Sarikaya, C. Tamerler, A. K.-Y. Jen, K. Schulten, F. Baneyx, *Nat. Mater.* **2003**, *2*, 577.
[9] P. Laaksonen, G. R. Szilvay, M. B. Linder, *Trends Biotechnol.* **2012**, *30*, 191.
[10] S. Mann. *Biomineralization: Principles and Concepts in Bio-Inorganic Materials Chemistry*, Oxford University Press, Oxford **2001**.
[11] A. Rao, J. K. Berg, M. Kellermeier, D. Gebauer, *Eur. J. Mineral.* **2014**, *26*, 537.
[12] M. Rodahl, F. Höök, C. Frederiksson, C. A. Keller, A. Krozer, P. Brzezinski, P. Voinova, B. Kasemo, *Faraday Discuss.* **1997**, *107*, 229.
[13] R. L. Brutchey, D. E. Morse, *Chem. Rev.* **2008**, *108*, 4915.
[14] K. Shimizu, J. Cha, G. D. Stucky, D. E. Morse, *Proc. Natl. Acad. Sci. USA* **1998**, *95*, 6234.
[15] J. L. Sumerel, W. Yang, D. Kisailus, J. C. Weaver, J. H. Choi, D. E. Morse, *Chem. Mater.* **2003**, *15*, 4804.
[16] L. A. Bawazer, J. Ihli, M. A. Levenstein, L. J. C. Jeuken, F. C. Meldrum, D. G. G. McMillan, *J. Mater. Chem. B* **2018**, *6*, 3979.
[17] G. Sauerbrey, *Z. Phys.* **1959**, *155*, 206.
[18] M. V. Voinova, M. Rodahl, M. Jonson, B. Kasemo, *Phys. Scr.* **1999**, *59*, 391.
[19] T. Shagawa, H. Torii, F. Kato, H. Ogi, M. Hirao, *Jpn. J. Appl. Phys.* **2015**, *54*, 096601.
[20] C. Zhou, J. Friedt, A. Angelova, K. Choi, W. Laureyn, F. Frederix, L. A. Francis, A. Campitelli, Y. Engelborghs, G. Borghs, *Langmuir* **2004**, *20*, 5870.
[21] R. Krause-Rehberg, H. S. Leipner. *Positron Annihilation in Semiconductors - Defect Studies*, Springer Verlag, Berlin, **1999**.
[22] A. van Veen, H. Schut, J. de Vries, R. A. Hakvoort, M. R. IJpma, *AIP Conf. Proc.* **1991**, *218*, 171.
[23] P. Schultz, K. G. Lynn, *Rev. Mod. Phys.* **1988**, *60*, 701.
[24] H. Schut, A. van Veen, *Appl. Surf. Sci.* **1995**, *85*, 225.
[25] Z. Ghorannevis, E. Akbernejad, M. Ghoranneviss, *J. Theor. Appl. Phys.* **2015**, *9*, 285.
[26] L. Kerkache, A. Layadi, E. Dogheche, D. Rémiens, *J. Phys. D: Appl. Phys.* **2006**, *39*, 184.
[27] F. Tuomisto, I. Makkonen, *Rev. Mod. Phys.* **2013**, *85*, 1583.
[28] D. Bochert, *Diploma Thesis*, Universität der Bundeswehr München, München, Germany **2004**.
[29] W. Egger, P. Sperr, G. Kögel, M. Wetzel, H.-J. Gudladt, *Appl. Surf. Sci.* **2008**, *255*, 209.
[30] A. Uedono, K. Ikeuchi, T. Otsuka, K. Yamabe, K. Eguchi, M. Takayanagi, T. Ohdaira, M. Muramatsu, R. Suzuki, A. S. Hamid, T. Chikyow, *Appl. Phys. Lett.* **2006**, *88*, 171912.
[31] A. Nakamoto, M. Saito, T. Yamasaki, M. Okamoto, T. Hamada, T. Ohno, *Jpn. J. Appl. Phys.* **2008**, *47*, 2213.
[32] P. R. Guagliardo, E. R. Vance, Z. Zhang, J. Davis, J. F. Williams, S. N. Samarin, *J. Am. Ceram. Soc.* **2012**, *95*, 1727.
[33] S. Ghosh, G. G. Khan, K. Mandal, A. Samanta, P. M. G. Nambissan, *J. Phys. Chem. C* **2013**, *117*, 8458.
[34] H. Luitel, A. Sarkar, M. Chakrabarti, S. Chattopadhyay, K. Asokan, D. Sanyal, *Nucl. Instrum. Methods Phys. Res., Sect. B* **2016**, *379*, 215.

**ADVANCED
SCIENCE NEWS**

www.advancedsciencenews.com

**ADVANCED
SUSTAINABLE
SYSTEMS**

www.advsustainsys.com

[35] J. Yan, G. Wu, N. Guan, L. Li, Z. Li, X. Cao, *Phys. Chem. Chem. Phys.* **2013**, *15*, 10978.

[36] H. Murakami, N. Onizuka, J. Sasaki, N. Thonghai, *J. Mater. Sci.* **1998**, *33*, 5811.

[37] S. J. Tao, *J. Chem. Phys.* **1972**, *56*, 5499.

[38] M. Eldrup, D. Lightbody, J. N. Sherwood, *Chem. Phys.* **1981**, *63*, 51.

[39] D. W. Gidley, W. E. Frieze, T. L. Dull, A. F. Yee, E. T. Ryan, H.-M. Ho, *Phys. Rev. B* **1999**, *60*, R5157.

[40] P. Semalti, S. N. Sharma, *J. Nanosci. Nanotechnol.* **2020**, *20*, 3647.

[41] M. R. Narayan, *Renewable Sustainable Energy Rev.* **2012**, *16*, 208.

[42] Md. K. Nazeeruddin, E. Baranoff, M. Grätzel, *Sol. Energy* **2011**, *85*, 1172.

[43] F. Bella, C. Gerbaldi, C. Barolob, M. Grätzel, *Chem. Soc. Rev.* **2015**, *44*, 3431.

[44] P. Sperr, W. Egger, W. Kögel, G. Dollinger, C. Hugenschmidt, R. Repper, C. Piochacz, *Appl. Surf. Sci.* **2008**, *255*, 35.

[45] C. Hugenschmidt, B. Löwe, J. Mayer, C. Piochacz, P. Pikart, R. Repper, M. Stadlbauer, K. Schreckenbach, *Nucl. Instrum. Methods Phys. Res., Sect. A* **2008**, *593*, 616.

2000003 (12 of 12)